Chemical Papers (2023) 77:1619–1630
https://doi.org/10.1007/s11696-022-02580-8

ORIGINAL PAPER

# Electrochemical sensing of caffeine in real-life samples and its interaction with calf thymus DNA

**Alper Fitoz**[1] · **Zehra Yazan**[1]

Received: 28 August 2022 / Accepted: 6 November 2022 / Published online: 14 November 2022
© Institute of Chemistry, Slovak Academy of Sciences 2022

## Abstract

This paper presents a bare pencil graphite electrode (bPGE) utilized for the electrochemical determination of caffeine (CAF). The electrochemical behavior of CAF was examined with the cyclic voltammetry technique. The oxidation of CAF is an irreversible and diffusion-controlled mechanism on the bPGE surface. The 0.1 M $H_2SO_4$ solution produced the highest oxidation peak currents of CAF using differential pulse (DPV) and square wave (SWV) voltammetry techniques. The pH of the $H_2SO_4$ solution was examined to determine its optimum value. The pH 1.0 value obtained the highest peak currents with both techniques. DPV and SWV methods achieved electrochemical determination of CAF with 30.0–1000.0 µM, and 10–1000 µM linear working ranges, respectively. LOD values for DPV and SWV techniques are 8.84 µM, and 9.36 µM, respectively. The developed methods were tested with real samples (cola and energy drink) and interference studies. DPV and SWV methods achieved real sample analysis with recovery values of between %95.6 and %103.8. Besides, the DNA binding constant of CAF was scanned via the in-solution method with both techniques. The calculated binding constants for DPV and SWV are $4.52 \times 10^3$ $M^{-1}$ and $8.64 \times 10^3$ $M^{-1}$, respectively, indicating that the interaction between DNA and CAF is facilitated by weak electrostatic forces.

### Graphical abstract

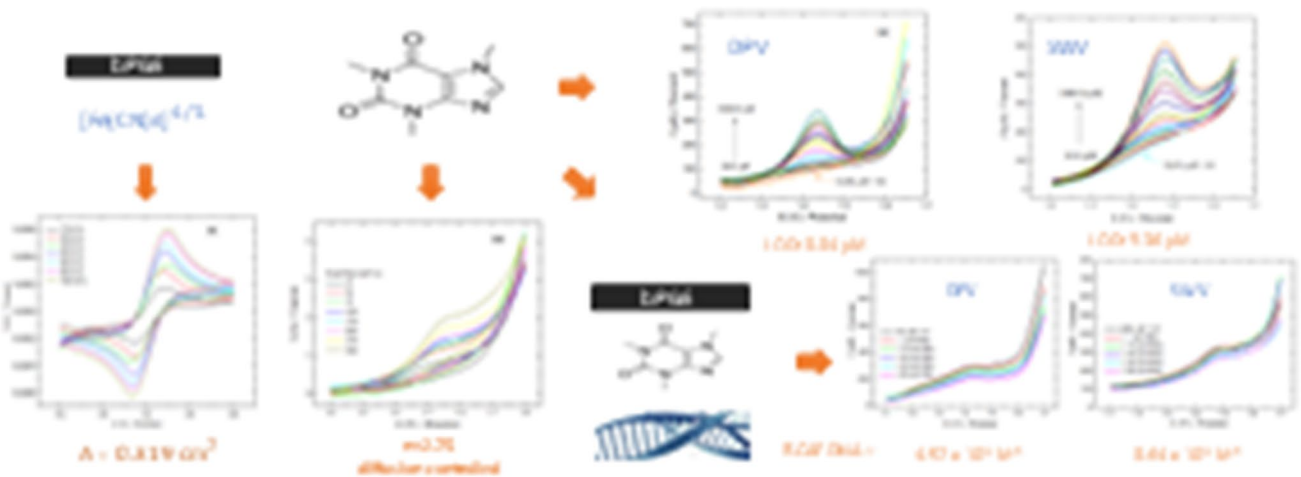


**Keywords** Caffeine · Voltammetry · PGE · DNA interaction · Binding constant

✉ Zehra Yazan
zdurmus@science.ankara.edu.tr

[1] Department of Chemistry, Faculty of Science, Ankara University, 06560 Ankara, Turkey

## Introduction

Deoxyribonucleic acid (DNA) is a magical structure for all living organisms due to its features, including carrying hereditary information, copying genetic information, and executing the transcription process and syntheses of proteins and enzymes (Erdem and Ozsoz 2002). The double-helix structure of DNA can be disrupted by radiation or through the binding of chemical or biological ligand molecules (Choi and Lee 2022). The damaged and broken structure of DNA cannot perform its normal functions and causes various hereditary diseases in living things (Li et al. 2007; Caldecott et al. 2022). Consequently, drug-agent and food-derived molecules binding to DNA have become increasingly important in recent years (Sirajuddin et al. 2013). These observations could improve our understanding of mutations and the development of efficient drugs for the treatment of DNA-related disorders.

Caffeine (IUPAC name: 1,3,7-Trimethylpurine-2,6-dione), also known as 1,3,7-methylxanthine, is an essential purine molecule. CAF is commonly used in the culinary and pharmaceutical industries, particularly in high-content CAF drinks (Ly et al. 2004). Besides, CAF is a naturally occurring active alkaloid found in coffee and tea plants. CAF has several pharmacological effects on the central nervous system, diuresis, and cardiovascular system (Klevebrant and Frick 2022; Aklilu et al. 2008; Zhang et al. 2011). CAF boosts alertness while lowering fine motor coordination at moderate dosages. It also causes dizziness, sleeplessness, headaches, and irritability (Habibi et al. 2012). Over the last decade, people of all ages have used energy drinks with a high CAF content (Berman et al. 2022). According to published statistics, the average CAF consumption per individual is 70 mg per day. Depending on the nation, this value can be interchanged (Vieira et al. 2022).

CAF's chemical structure is similar to other N-methyl xanthine derivatives (theophylline, theobromine, etc.) (Fitoz et al. 2021) and purine molecules, including uric acid, adenine, and guanine, etc. (Legraverend and Grierson 2006). Purine nucleotide metabolism may be compromised as a result of purine interactions with DNA (Neef et al. 2012). The term "intercalation" describes the DNA interaction of small aromatic molecules. Three different processes can lead to intercalation: groove bonding, non-specific electrostatic binding with a negatively charged nucleic acid-phosphate complex, and binding between DNA base pairs in a double-helix structure (Mukherjee and Sasikala 2013). Scanning the DNA interactions of these biomolecules that interact with DNA using widely established diets, drugs, and bodily fluids could therefore help identify the effects of mutation on DNA structure.

Considering CAF is an essential biomolecule due to its usage in both the food and pharmaceutical industries, it will be essential to investigate how it interacts with ds-DNA using voltammetric techniques and a bare PGE (bPGE). Furthermore, the literature survey reveals that the electrochemical interaction of CAF with DNA has never been examined. As a result, this is the first study to use electrochemical techniques to calculate the binding constant of the CAF–DNA complex. The CAF–DNA interaction has been studied in the literature using UV spectroscopy, and the findings demonstrate that weak electrostatic forces regulate this interaction (Nafisi et al. 2008; Johnson et al. 2012).

Due to the obvious enormous use of high-content CAF beverages across the world, a low-cost, rapid, and direct assessment technique is required. Chromatography (Soto et al. 2022, Ferky et al. 2022) and spectroscopy (Shokrzadeh et al. 2022; Tran et al. 2022) are useful techniques, although they have significant drawbacks. The former produces hazardous waste solutions, while the latter has an issue with interference (Svorc 2013). Electrochemical techniques, on the other hand, have a number of advantages, including cost-effectiveness, ease of operation, and application procedures (Ferrag et al. 2020; Jadon et al. 2016). Electrochemical methods have also succeeded in scanning the DNA interaction of small aromatic molecules (Rauf et al. 2005; Bayraktepe 2020).

Researchers have employed glassy carbon (Torres et al. 2014), carbon paste (Mahanthappa et al. 2016), carbon-ceramic (Habibi et al. 2014), pencil graphite (Gowda and Nandibewoor 2014), and boron-doped diamond electrodes (Eisele et al. 2017) to quantify the caffeine content of a variety of real-world samples. Except for pencil graphite electrodes (PGEs), these electrodes involve time-consuming preparation processes and are not cost-effective. Due to their inexpensive cost, disposable nature, and commercial availability in stationary stores, PGEs are unique electrodes (Fitoz et al. 2021; Kawde et al. 2016; Mahnashi et al. 2020). CAF has been electrochemically detected in the literature (Aklilu et al. 2008; Zhang et al. 2011; Habibi et al. 2012; Zereykaya et al. 2020) due to its widespread demand and numerous applications. While these methods result in lower LOD values, they need time-consuming pre-processing (modification or surface treatments). In this study, we focused on developing analysis methods that used a single calibration curve and wider linear working ranges without any pre-processing. Ultimately, the DPV and SWV techniques were successful in determining CAF in real-world samples (energy drink and cola).

In this paper, we used a disposable bPGE to develop two techniques (DPV and SWV) for determining CAF in real-world samples without any pre-treatment or modification step. The influence of CAF's oxidation peak current on several electrolyte solutions was investigated for this purpose.

The pH change of a 0.1 M $H_2SO_4$ electrolyte solution was then studied, and the optimum value was determined to be pH: 1.0. Furthermore, the influence of concentration on CAF anodic peak currents was examined under optimum conditions. For high-content CAF drinks, the two procedures presented provided rapid and consistent results. The CAF–DNA interaction was investigated by calculating the binding constant of the CAF–DNA complex using the decrease in the oxidation peak currents of CAF after the addition of DNA into the electrochemical cell. Calculated binding constants for both DPV and SWV revealed that the interaction is formed via weak electrostatic interactions, according to the calculated binding constants. In addition, scan rate analysis conducted in the absence and presence of DNA to calculate kinetic parameters including the diffusion coefficient and the standard heterogeneous rate constant to demonstrate the formation of CAF–DNA complex.

## Experimental

### Materials

Sigma-Aldrich Company provided xanthine (XT, % 99), theophylline (TP, % 99), theobromine (TB, % 98), caffeine (CAF, % 99), uric acid (UA, % 99), L-glycine (% 99), nitric acid (% 65), sulfuric acid (% 95–97), phosphoric acid (% 85–88), acetic acid (% 100), boric acid (% 99.5). Perchloric acid (60%) and sodium hydroxide (97%) were also acquired from the MERC Company.

Just before the voltammetric measurements, a stock solution of CAF (19.02 mg CAF/10 mL = $10^{-2}$ mol CAF/L) was prepared in double-distilled water. We also employed $10^{-3}$ and $10^{-5}$ M CAF stock solutions in our calibration investigations. These solutions were prepared by diluting the $10^{-2}$ M CAF solution.

5 mg of ds-DNA (Calf thymus) was mixed with 5 mL of double-distilled water to produce the DNA stock solution. Then, UV-spectroscopy (max: 260 nm) was used to determine the concentration of this solution ($2.0 \times 10^{-3}$ mol/L) (Bayraktepe 2020).

### Instrumentation

The investigation was completed utilizing a CHI760B Potentiostat/Galvanostat working station and a BAS C3 cell stand for voltammetric measurements (CV, DPV, and SWV). Pt wire (BASi MW-1032) was used as the auxiliary electrode, Ag/AgCl (BASi MF-2052) was used as the reference electrode, and pencil graphite electrode (PGE) was used as the working electrode. PGEs were bought at a local stationary store (Faber Castel 0.7 × 75 mm). To assure inertness, $N_2$(g) was fed through the electrochemical cell before all experiments.

CV measurements were applied with these optimum conditions; potential scan for CAF: initial potential: 1.2 V, high potential: 1.8 V, and final potential: 1.2 V.

DPV measurements were applied with these optimum conditions: potential scan for CAF: 1.2–1.7 V, potential increase: 0.004 V, amplitude: 0.05 V, sampling width: 0.0167 s., and pulse period: 0.5 s.

SWV measurements were applied with these optimum conditions: potential scan for CAF: 1.2–1.7 V, potential increase: 0.004 V, amplitude: 0.025 V, frequency: 15 Hz ($s^{-1}$).

A mpMINIpure device generates double-distilled water. Using a HANNA HI2211 pH/ORP meter with 0.01, 0.1, and 1.0 M HCl and NaOH solutions, the pH values of working solutions were adjusted.

### Interference, reproducibility, repeatability, and stability studies

Interference tests were performed with a solution containing 50 µM CAF. The electrochemical cell was then filled with interfering agents in 1:1, 1:2, 1:3, 1:4, and 1:5 ratios, including XT, TP, TB, UA, AA, L-Glycine, and $Na_3PO_4$. CAF oxidation current changes were studied after this addition, and tolerance limits were calculated. For this purpose, the tolerance limit was set at a %5 error.

The oxidation peak currents of the CAF were tested with five identical pencil graphite electrodes to assess the repeatability of the used sensor (bPGE). With each sensor, five samples were recorded, and the %RSD values were determined over the CAF oxidation current values.

Five measurements were conducted using a pencil graphite electrode to assess the repeatability of the used sensor (bPGE), and the oxidation peak currents of the CAF were evaluated. For the CAF oxidation current values, the %RSD values were determined.

The stability of the bPGE was tested using the CV method after 50 cycles. The %RSD of the reduction and oxidation peak currents of the $[Fe(CN)_6]^{4-/3-}$ standard redox probe was determined for this purpose and recorded at a scan rate of 100 mV/s in the potential range of − 0.2 to + 0.6 V and then to − 0.2 V.

### Real sample analysis

The established procedures were put to the test using samples of cola (Coca-Cola) and energy drink (Red Bull). The caffeine index in both samples is 150 mg/mL. Before the testing, the carbonated beverage samples were mixed for 10 min to release gases. This solution was employed as a stock solution. The electrochemical cell received a certain

amount of stock solution. The cell was then filled with $H_2SO_4$ (pH: 1.0) to a volume of 10.0 mL. DPV and SWV measurements were performed after a certain amount of CAF was spiked into the electrochemical cell. Eventually, the recovery (%) and relative standard deviation (%) values were calculated. The results were calculated at the 95% confidence level by averaging the three measurements. The recovery values (%) were calculated as follows:

$$\%\text{Recovery} = \frac{C_2}{C_1} \times 100 \tag{1}$$

here $C_2$ represents the measured concentration, and $C_1$ represents the spiked or known concentration. %RSD values were calculated as follows:

$$\%\text{RSD} = \frac{s}{\bar{x}} \times 100 \tag{2}$$

here $s$ represents the standard deviation of three measurements, and $\bar{x}$ represents the average of three measurements.

### The evaluation of DNA interaction

The in-solution approach was used to assess CAF's DNA interaction. First, we determined the interaction time between CAF and DNA. As a consequence of the measurements, this value was observed to be 150 s. The change in the oxidation peak of caffeine was examined by applying a certain amount of DNA to the electrochemical cell. CAF oxidation currents decreased after DNA was added to the electrochemical cell. Investigating the scan rate analysis, the diffusion coefficient value ($D$) and the standard heterogeneous rate constant ($k^0$) value of CAF was calculated in the absence and presence of DNA. $D$ values were calculated using the slope of $i_{pa}$–$v^{1/2}$ plot and Randles–Sevcik equation (Eq. 7). $k0$ values were calculated using the slope of $E_{pa}$–ln $v$ plots and the Laviron equation as follows:

$$E_{pa} = E^0 + \left(\frac{RT}{\alpha nF}\right) \ln\left(\frac{RTk^0}{\propto nF}\right) \ln v \tag{3}$$

$E_{pa}$ (V), $E^0$ (V), $R$ (8.314 J/K mol), $T$ (Kelvin), $n$, (C/mol), $^0$, and $v$ (V/s) denote the oxidation potential, formal potential, ideal gas constant, temperature, electron transfer coefficient, transferred electron number, Faraday constant, standard heterogeneous rate constant, and scan rate, respectively (Ilager et al. 2022).

The general reaction between CAF and DNA is represented below:

$$\text{mCAF} + \text{DNA} \leftrightarrow [\text{mCAF} - \text{DNA}] \tag{4}$$

The relation between anodic peak currents and DNA concentration is given in the literature as follows:

$$\log\left[\frac{i_{\text{CAF–DNA}}}{i_{\text{CAF}} - i_{\text{CAF–DNA}}}\right] = \log K_{\text{CAF–DNA}} + m \log\left[\frac{1}{C_{\text{DNA}}}\right] \tag{5}$$

here $m$, $K_{\text{CAF–DNA}}$, $i_{\text{CAF}}$, and $i_{\text{CAF–DNA}}$ represent the binding ratio, the binding constant of the CAF–DNA complex, the anodic peak current of CAF in DNA-free solution, and the anodic peak currents of CAF in DNA-added solution (Bayraktepe 2020), respectively. The DNA solution was added to the electrochemical cell with varying concentrations in order to demonstrate the linearity between $\log[1/C_{\text{DNA}}]$ and the decrease in the oxidation peak currents of CAF ($\log [[i_{\text{CAF–DNA}}]/[i_{\text{CAF}} - i_{\text{CAF–DNA}}]]$). After determination of $K_{\text{CAF–DNA}}$, we calculated the standard Gibbs free energy change ($\Delta G^0$) to determine the binding nature (spontaneous, etc.). For this, we used the following thermodynamic equation:

$$\Delta G^0 = -\text{RT} \ln K_{\text{CAF–DNA}} \tag{6}$$

here $R$, $T$, and $K_{\text{CAF–DNA}}$ are the ideal gas constant (J/K mole), the absolute temperature (Kelvin, K), and the binding constant of the CAF–DNA complex (Yazan et al. 2020), respectively.

## Results and discussion

### Electrochemical performance of bPGE

The CV technique was used to assess the electrochemical performance of bPGE with a 5.0 mM $[Fe(CN)_6]^{4-/3-}$ redox probe at various scan rates ($v$: 10, 20, 40, 50, 60, 80, and 100 mV/s). These voltammograms are displayed in Fig. S1. As the scan rate increases, the peak currents of $[Fe(CN)_6]^{4-/3-}$ increase, and the anodic peak potentials shift more positive values, as seen in the voltammograms. The Randles–Sevcik equation explains the relation between $v^{1/2}$ and $i_{pa}$ as follows:

$$i_{pa} = \left(2.687 \times 10^5\right) n^{\frac{3}{2}} \cdot \text{A.D}^{1/2} \cdot \text{C.v}^{1/2} \tag{7}$$

here $i_{pa}$, $n$, A, D, C, and $v$ represent anodic peak current (ampere), number of transferred electrons, redox-active surface area ($cm^2$), diffusion coefficient ($cm^2/s$), concentration ($mol/cm^3$), and scan rate (V/s), respectively. The $D$ and $n$ values for $[Fe(CN)_6]^{4-/3-}$ are $7.6 \times 10^{-6}$ $cm^2/s$ and 1 (Bayraktepe et al. 2016), respectively. The linearity of the $i_{pa}$–$v^{1/2}$ plot ($i_{pa}$ (A) $= 1.180 \times 10^{-3}$ ($\pm 3.310 \times 10^{-5}$) $v^{1/2} + 1.214 \times 10^{-4}$ ($\pm 7.510 \times 10^{-6}$), $R^2 = 0.9953$) indicates that $[Fe(CN)_6]^{4-/3-}$ oxidates on the bPGE surface via a diffusion-controlled mechanism. Using the slope of the $i_{pa}$–$v^{1/2}$ curve and the Randles–Sevcik Equation together, the active surface area of bPGE was calculated as 0.319 $cm^2$.

The stability of bPGE was investigated using a 5.0 mM $[Fe(CN)_6]^{4-/3-}$ standard redox probe and a multi-scan (50 cycle, scan rate $v$: 100 mV/s) analysis. The calculated %RSD value is %3.42, representing excellent measurement stability.

## Electrolyte effect

The choice of electrolyte to utilize was studied using DPV and SWV methods prior to the research of the electrochemical behavior of CAF. As an electrolyte solution, 0.1 M solutions of $H_2SO_4$, HCl, $HClO_4$, and $HNO_3$ were investigated. Figure 1 exhibits DP and SW voltammograms of $10^{-4}$ M CAF in several electrolyte solutions. Considering that 0.1 M $H_2SO_4$ solution produced the highest anodic peak currents, it was selected as the electrolyte solution for further investigation.

## Electrochemical behavior of CAF on bPGE

The CV technique was used to evaluate the electrochemical behavior of CAF on the bPGE surface at various scan rates ($v$; 25, 50, 75, 100, 150, 200, 250, and 300 mV/s). CV voltammograms of CAF at various scan rates are represented in Fig. S2. CAF oxidizes irreversibly on the bPGE surface, as observed in these voltammograms. As the scan rate ($v$) increases, anodic peak currents ($i_{pa}$) increase while anodic peak potentials ($E_{pa}$) shift to more positive values (Fig. S2a).

For further evaluation, $i_{pa} - v^{1/2}$ (Fig. S2b), $\log i_{pa} - \log v$ (Fig. S2c), and $E_{pa} - \log v$ (Fig. S2d) plots of CAF were examined. The linearity of the $i_{pa}$–$v^{1/2}$ graph (Eq. 8) indicates that CAF oxidates on bPGE via a diffusion-controlled mechanism (Geto and Brett 2021). On the other hand, the slope of the $\log i_{pa} - \log v$ graph (Eq. 9) is 0.6, close to 0.5, indicating that the oxidation of CAF on bPGE is diffusion controlled on the bPGE surface (Anvari et al. 2021).

$$i_{pa}(\text{mA}) = 24.496v^{1/2}(\pm 0.652)\ (\text{mV/s})^{1/2} - 43.295(\pm 7.826),\ R^2 = 0.9958 \tag{8}$$

$$\log i_{pa}(\text{mA}) = 0.605\,(\pm 0.015)\ \log v(\text{mV/s}) + 1.085\,(\pm 0.031),\ R^2 = 0.9963 \tag{9}$$

The Laviron equation has been used in the literature to calculate the number of transferred electrons during the oxidation process. The equation is as follows:

$$E_{pa} = E^0 + \left(\frac{2.303\text{RT}}{\alpha nF}\right)\log\left(\frac{\text{RT}k^0}{\alpha nF}\right) + \left(\frac{2.303\text{RT}}{\alpha nF}\right)\log v \tag{10}$$

here $E_{pa}$, $R$, $T$, $F$, $n$, $k^0$, $v$, and $\alpha$ represent anodic peak potential (V), ideal gas constant (8.314 J/mol K), temperature (K), Faraday constant (96,485 C/mole), number of transferred electrons, heterogeneous rate constant, scan rate (V/s), and electron transfer coefficient, respectively. For an irreversible redox process, the α value is assumed to be 0.5 (Fitoz et al. 2021; Gowda and Nandibewoor 2014). The linearity between $E_{pa}$ and $\log v$ is as follows:

$$E_{pa}(V) = 0.043(\pm 0.001)\ \log v + 1.563(\pm 0.001),\quad R^2 = 0.9884 \tag{11}$$

We calculated CAF's number of transferred electrons on the bPGE surface as 2.75 (0.06) using Eq. 10 and the slope of the $E_{pa}$–$\log v$ plot (Eq. 11).

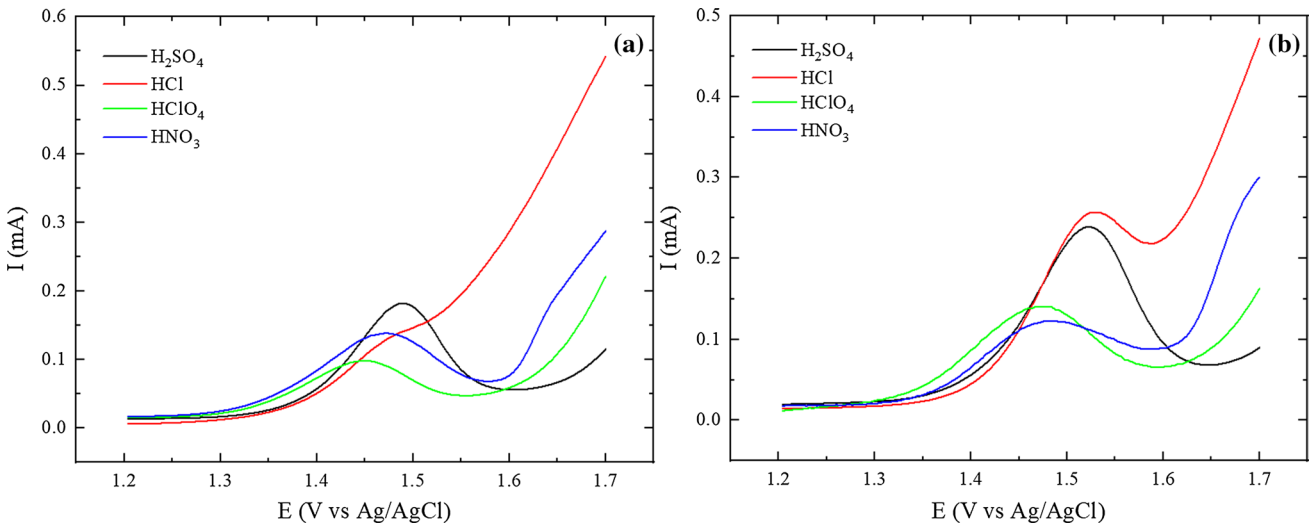


**Fig. 1** Effect of various electrolytes on the anodic peaks of $10^{-4}$ M CAF; **a** DP and **b** SW voltammograms

## pH effect

The pH value of the supporting electrolyte contributes significantly to the electrode reaction due to the involvement of protons in redox reactions. Using DPV and SWV techniques, the pH of the electrolyte solution (0.1 M $H_2SO_4$) was varied from 0.5 to 3.5, and the change in $E_{pa}$ and $i_{pa}$ was observed.

Figure 2 illustrates voltammograms and $E_{pa}$–pH plots (as an inset). At a pH of 1.0, both techniques exhibited a significant $i_{pa}$. As a result, this pH is chosen as the optimum value for both procedures.

The linearities between pH and $E_{pa}$ are represented below:

$$\mathrm{DPV}; E_{pa}(V) = 0.033\,(\pm 0.001)\,pH + 1.451\,(\pm 0.002),\quad R^2 = 0.9992 \tag{12}$$

$$\mathrm{SWV}: E_{pa}(V) = 0.047\,(\pm 0.002)\,pH + 1.473\,(\pm 0.003),\quad R^2 = 0.9983 \tag{13}$$

The slopes of the $E_{pa}$–pH plots for DPV and SWV were calculated as 0.033 and 0.047 V/pH. These findings support earlier studies, suggesting that CAF's oxidation process deviates from the Nernstian trend and involves a two-step, 4proton:4electron mechanism (Geto and Brett 2021; Patel et al. 2020; Svorc et al. 2018).

## Calibration studies

We investigated the association between CAF's $i_{pa}$ and concentration after setting optimum conditions (0.1 M $H_2SO_4$, pH: 1.0, other optimum conditions were stated in the experimental section). Figures 3 and 4 represent the voltammograms (a) and calibration plots (b) for DPV and SWV, respectively. As seen in the voltammograms, both methods increase $i_{pa}$ values as CAF concentration rises. The linear working ranges for DPV and SWV are 30.0–1000.0 M and 10.0–1000.0 M, respectively. The resulting calibration plots for DPV and SWV are as follows:

$$\mathrm{DPV}: i_{pa}(\mu A) = 0.206\,(\pm 0.003)\,C_{CAF}(\mu\mathrm{M}) - 5.390\,(\pm 1.352),\ R^2 = 0.9981 \tag{14}$$

$$\mathrm{SWV}: i_{pa}(\mu\mathrm{A}) = 0.261\,(\pm 0.003)\,C_{CAF}(\mu\mathrm{M}) + 3.815\,(\pm 1.607),\ R^2 = 0.9981 \tag{15}$$

LOD and LOQ values were calculated with 3 s/m and 10 s/m assumptions, respectively. The LOD and LOQ values were derived using assumptions of 3 s/m and 10 s/m, respectively. The slope of the calibration curve, or selectivity, and the standard deviation of the initial calibration points are represented by $m$ and $s$, respectively. Calculated LOD values for DPV and SWV techniques are 8.84 and 9.36 µM, respectively.

On the one hand, the SWV technique demonstrates more sensitivity to CAF and slightly wider linear working ranges. On the other hand, the DPV technique demonstrated a lower LOD value due to demonstrating a lower standard deviation value as shown in Table 1. A comparison of calibration parameters with the literature is given in Table 2. Individual (Ly et al. 2004; Aklilu et al. 2008; Zhang et al. 2011; Habibi et al. 2012; Zereykaya et al. 2020; Geto and Brett 2021; Svorc et al. 2018; Alizadeh et al. 2010; Rezaei et al. 2014) and simultaneous (Mekassa et al. 2017; Koçak et al. 2018; Bayraktepe et al. 2021; Sarakhman et al. 2022) analysis of

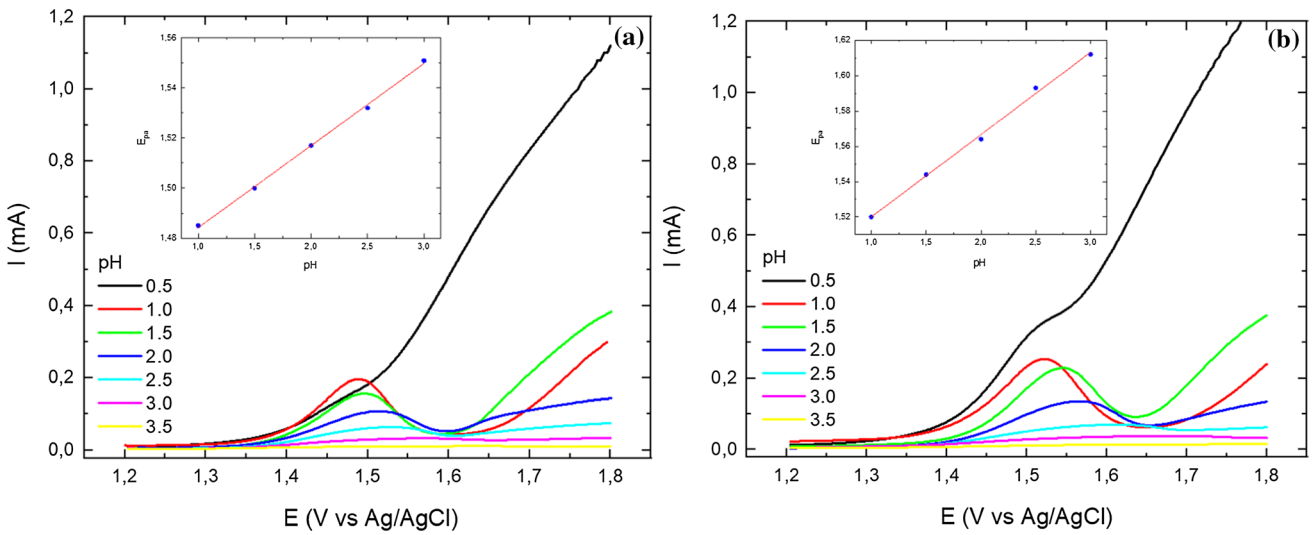


**Fig. 2** **a** DP and **b** SW voltammograms measured in various pH values (insets: $E_{pa}$–pH plot)

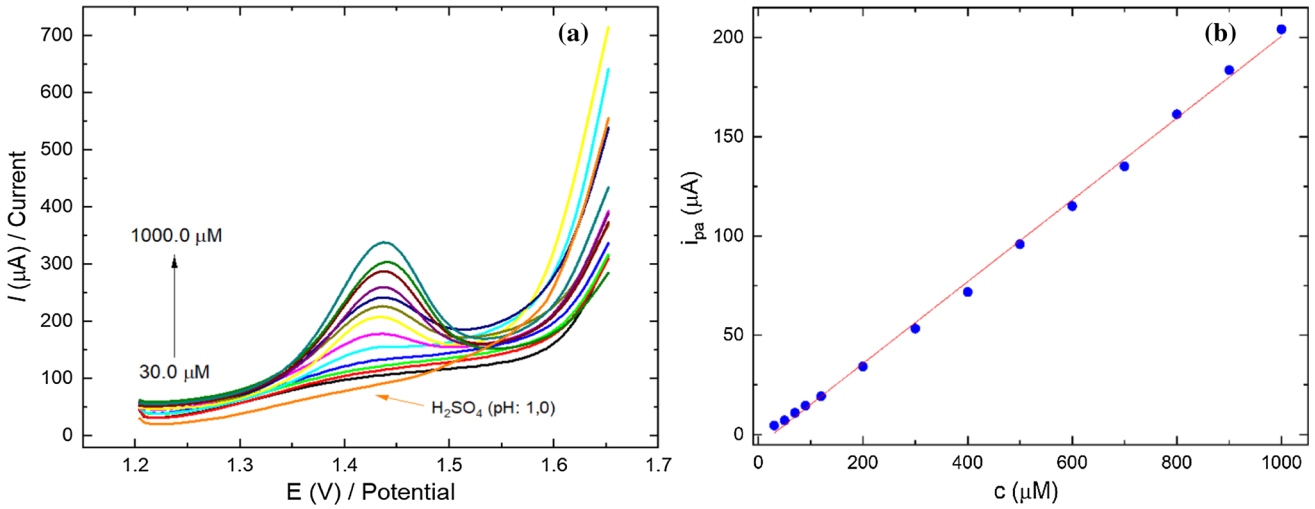


**Fig. 3** **a** DP voltammograms of CAF in various concentrations (30–1000 μM), **b** DPV calibration curve

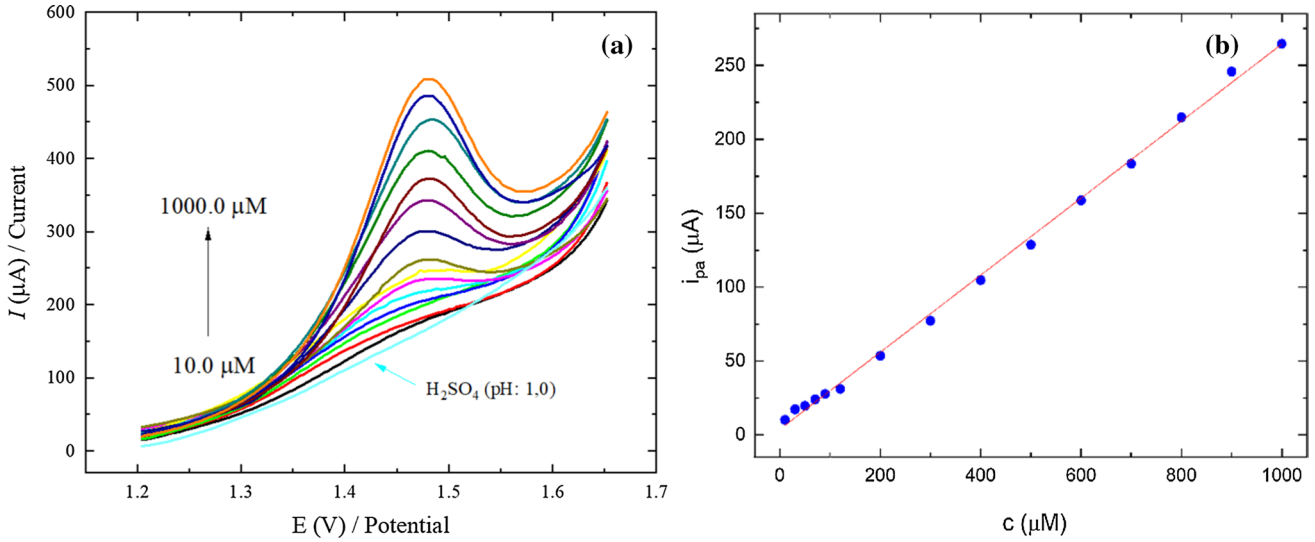


**Fig. 4** **a** SW voltammograms of CAF in various concentrations (10–1000 μM) and **b** SWV calibration curve

**Table 1** Comparison of calibration parameters obtained by DPV and SWV techniques with each other

| Parameters | DPV | SWV |
|---|---|---|
| Linear working range (μM) | 30.0–1000.0 | 10.0–1000.0 |
| Selectivity (Slope, m) | 0.206 (±0.003) | 0.261 (±0.003) |
| Intercept | −5.390 (±1.352) | +3.815 (±1.607) |
| $R^2$ | 0.9981 | 0.9981 |
| LOD | 8.84 | 9.36 |
| LOQ | 29.46 | 31.19 |
| Repeatability of peak currents (%RSD) | 4.64 | 5.68 |
| Reproducibility of peak currents (%RSD) | 3.55 | 3.91 |

**Table 2** Comparison of the analytical performance of bPGE with some previously reported literature

| Technique | Electrode | Linear working range | LOD | References |
|---|---|---|---|---|
| SWASV | bPGE | 0–500 mg/L | 9.2 mg/L | Ly et al. (2004) |
| SWV | BQ/GCE | 0–0.5 mM | 0.3 µM | Aklilu et al. (2008) |
| | | 0.5–8.0 mM | 5.1 µM | |
| DPASV | MWCNT-Nafion/GCE | 2.945–377 µM | 0.513 µM | Zhang et al. (2011) |
| | | 377.0–2356.0 µM | | |
| DPV | SWCNT/CCE | $2.5\times10^{-7}$–$1.0\times10^{-4}$ M | $1.2\times10^{-7}$ M | Habibi et al. (2012) |
| DPV | Poly(7A4HN2SA)/GCE | 10–500 µM | 0.23 µM | Geto and Brett (2021) |
| DPV | BDDE | 0.40–25.0 µM | 150 nM | Svorc et al. (2012) |
| DPV | MIP/CPE | 0.06–25.0 µM | 15.0 nM | Alizadeh et al. (2010) |
| SWV | MIP/PGE | 0.002–1.0 nM | 0.9 nM | Rezaeş et al. (2014) |
| AdsDPV | bPGE | 2.36 -1000.0 µM | 0.71 µM | Zereykaya et al. (2020) |
| AdsSWV | | 3.69–1600 µM | 1.11 µM | |
| SWV | P(L-Asp)/f-MWCNTs/GCE | 1.0–150.0 µM | 0.28 µM | Mekassa et al. (2017) |
| DPV | 2eOHMnPc-CNT/GCE | 0.2–100.0 µM | $5.0\times10^{-8}$ M | Koçak et al. (2018) |
| | | 2.0 200.0 µM | $3.0\times10^{-7}$ M | |
| DPV | GrRAC-70% | 2.94–1000.0 µM | 2.94 µM | Monteiro et al. (2019) |
| DPV | AuNP/p(L-met)/PGE | 8.3–2000.0 µM | 2.50 µM | Bayraktepe et al. (2021) |
| SWV | PdNPs/GPE | 25–190 µmol $L^{-1}$ | 3.9 µmol $L^{-1}$ | Wong et al. (2021) |
| DPV | BDDE | 4.6–97.5 µM | 2.1 µM | Sarakhman et al. (2022) |
| SWV | | 9.2–95.0 µM | 4.6 µM | |
| DPV | bPGE | 30.0–1000.0 µM | 8.84 µM | This work |
| SWV | bPGE | 10.0–1000.0 µM | 9.36 µM | This work |

*bPGE* bare pencil graphite electrode, *BQ/GCE* 1,4-benzoquinone modified glassy carbon electrode, *MWCNT-Nafion/GCE* multi-walled carbon nanotube modified GCE, *SWCNT/CCE* single-walled carbon nanotube modified carbon ceramic electrode, *Poly(7A4HN2SA)/GCE* 7-amino-4-hydroxynaphthalene-2-sulfonic acid modified GCE, *MIP/CPE* molecularly imprinted polymer modified carbon paste electrode, *MIP/PGE* molecularly imprinted polymer modified PGE, *PdNPs/GPE* graphite pencil electrode modified with palladium nanoparticles, GrRAC-70%; cork modified graphite electrode

CAF has been applied at remarkably low LOD values. Some of these papers include time-consuming and costly modification processes or highly expensive electrodes. On the other hand, some of these papers include time-consuming pre-treatment processes. Our work group's latest study for individual analysis of CAF (Zereykaya et al. 2020) includes time-consuming pre-treatment processes. Consequently, our calibration methods do not achieve the lowest LOD value despite achieving slightly wider linear working ranges and single calibration equations with a significantly more cost-effective electrode without any modification and pre-treatment applications.

## Interference, reproducibility, and repeatability studies

The interference effect of some organic and inorganic species on the developed calibrations was examined on the effect of CAF anodic peak currents. XT, TP, and TB are commonly encountered in beverage samples together. The tolerance limit was expressed as the minimum concentration value with a relative error of less than 5%. The results are represented in Table 3. TB molecule interfered with the anodic peak current of CAF at a 1:1 ratio. This outcome may be because the two molecules have similar chemical structures and so the oxidation peaks overlap with each other (Nia et al. 2021).

**Table 3** Tolerance ratio of interfering agents on the electrochemical determination of CAF with DPV and SWV methods

| Interfering agents | Tolerance limits | | Error (%) | |
|---|---|---|---|---|
| | DPV | SWV | DPV | SWV |
| XT | 1:3 | 1:3 | −4.44 | −4.97 |
| TP | 1:2 | 1:2 | −4.58 | −4.77 |
| TB | 1:1 | 1:1 | +49.87 | +51.36 |
| UA | 1:3 | 1:3 | −4.72 | −4.93 |
| L-Glycine | 1:4 | 1:4 | −4.63 | −4.81 |
| $Na_3PO_4$ | 1:2 | 1:2 | +4.23 | +4.46 |

The reproducibility and repeatability of bPGE were investigated by evaluation of the oxidation currents of CAF. Calculated %RSD values are represented in Table 1. The bPGE

showed excellent reproducibility toward the CAF oxidation peaks with both DPV and SWV techniques. In the repeatability tests, the DPV technique presented excellent results, while the SWV technique achieved a %RSD value of just over 5%, indicating that the SWV technique has good repeatability against the CAF oxidation peak current.

## Real sample analysis

To test the developed methods, we selected two highly CAF-content real-world samples. The stock solutions for these samples were prepared according to the experimental section. We measured CAF content with the direct addition of real samples and spiked three different standard additions in the electrochemical cell. Consequently, we calculated recovery (%) and % RSD for each addition. The resulting recovery values are represented in Table 4 for DPV and SWV, and the related voltammograms are represented in Fig. S3. These results demonstrate that DPV and SWV methods effectively select CAF in two different media. Rapid and accurate determination of CAF in beverages with high caffeine content was achieved without any pre-treatment or surface modification or extra standard addition procedure.

## Interaction of CAF with ds-DNA

To demonstrate the formation of the CAF–DNA complex, scan rate analysis was performed using the CV technique (Fig. S4). The diffusion coefficient (D) and standard heterogeneous rate constant ($k^0$) were calculated using the $i_{pa}$–$v^{1/2}$ and $E_{pa}$–ln $v$ (Fig. S4b) plots (Eq. 16). $D$ was calculated in the absence of DNA as $3.93\times10^{-9}$ $cm^2/s$ using the slope of the $i_{pa}$–$v^{1/2}$ plot and the Randles–Sevcik equation (Eq. 7), and $k^0$ was calculated as 0.777 $s^{-1}$ using the slope of the $E_{pa}$–ln $v$ plot and the Laviron equation (Eq. 3).

$$E_{pa}(V) = 0.0188\,(\pm0.0008)\,\ln v + 1.563\,(\pm0.002),\quad R^2 = 0.9884 \tag{16}$$

In the presence of ds-DNA, $i_{pa}$–$v^{1/2}$ and $E_{pa}$–ln $v$ plots of CAF were applied to $D$ and $k^0$ values. The linearities of $i_{pa}$–$v^{1/2}$ (Fig. S4c) and $E_{pa}$–ln $v$ (Fig. S4d) are represented by the following equations:

$$i_{pa}(mA) = 15.686v^{1/2}(\pm0.690)\ (mV/s)^{1/2} - 2.771\,(\pm8.278),\ R^2 = 0.9885 \tag{17}$$

$$E_{pa}(V) = 0.037\,(\pm0.001)\,\ln v + 1.642\,(\pm0.004),\quad R^2 = 0.9897 \tag{18}$$

$D$ and $k^0$ values were calculated as $1.61\times10^{-9}$ $cm^2/s$ and 0.608 $s^{-1}$, respectively. Reduced results for $D$ and $k^0$ values represent the formation of the CAF–DNA complex.

DNA interaction via CAF was investigated under optimized conditions with the in-solution method by DPV and SWV techniques. Measurements were applied after a certain interaction time (150 s.). Figure 5 represents DP and SW voltammograms, as well as log [1/[DNA]]– log [[iCAF-DNA]/[iCAF-DNA] plots (as insets). We calculated $K_{CAF–DNA}$ from the intercepts of the log [1/[DNA]]–log $[[i_{CAF–DNA}]/[i_{CAF} - i_{CAF\text{-}DNA}]]$ plots via Eq. 5. These linear relations are as follows:

**Table 4** Recovery results for DPV and SWV techniques in two real-world samples

| Sample | Declared (μM) | Added sample (mL) | Found (μM) | Recovery (%) | RSD (%) | Spiked (μM) | Found (μM) | Recovery (%) | RSD (%) |
|---|---|---|---|---|---|---|---|---|---|
| *DPV* | | | | | | | | | |
| Coca-Cola | 772 | 1 | 78.00 ± 2.86 | 101 | 3.67 | 20 | 97.96 ± 3.68 | 103.8 | 3.76 |
| | | | | | | 40 | 116.7 ± 5.78 | 99.6 | 4.95 |
| | | | | | | 50 | 127.8 ± 6.11 | 99.6 | 4.78 |
| Red-Bull | 772 | 0.6 | 45.70 ± 1.75 | 98.7 | 3.83 | 10 | 54.20 ± 1.36 | 96.2 | 2.51 |
| | | | | | | 20 | 63.39 ± 2.93 | 95.6 | 4.62 |
| | | | | | | 40 | 82.93 ± 4.13 | 96.1 | 4.98 |
| *SWV* | | | | | | | | | |
| Coca-Cola | 772 | 0.5 | 37.67 ± 1.85 | 97.5 | 4.91 | 20 | 60.96 ± 2.81 | 104 | 4.61 |
| | | | | | | 40 | 79.44 ± 3.87 | 101.1 | 4.87 |
| | | | | | | 50 | 85.32 ± 4.13 | 96.3 | 4.84 |
| Red-Bull | 772 | 0.3 | 23.77 ± 1.12 | 102.6 | 4.71 | 10 | 32.41 ± 1.44 | 97.7 | 4.44 |
| | | | | | | 20 | 41.87 ± 2.93 | 97 | 4.62 |
| | | | | | | 40 | 63.55 ± 3.17 | 100.6 | 4.98 |

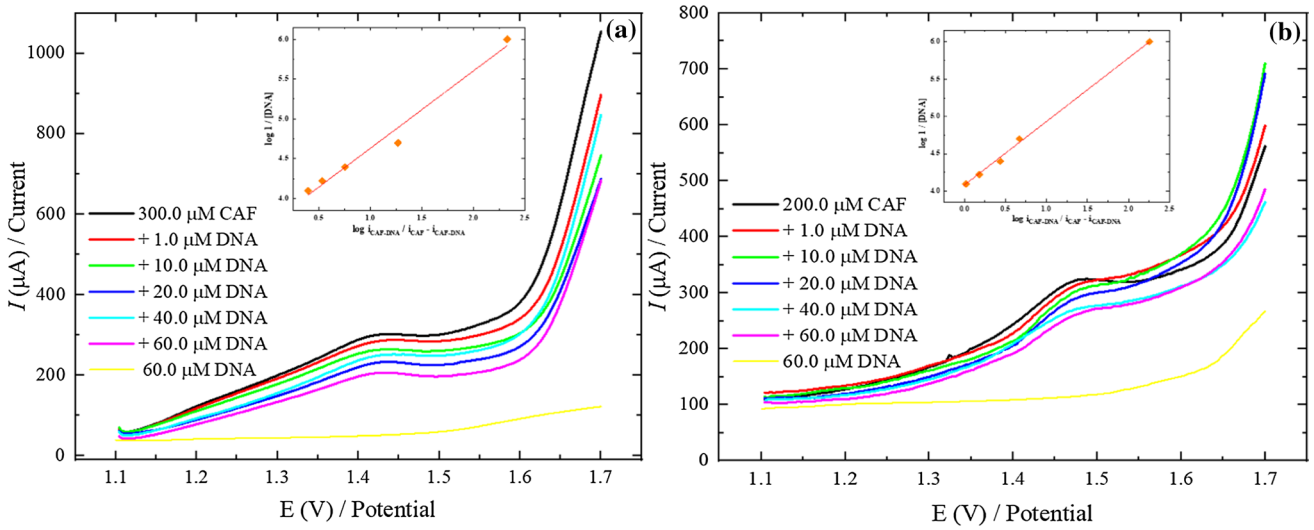


**Fig. 5** **a** DP and **b** SW voltammograms of CAF and DNA interaction (insets: log 1/[DNA] – log $[i_{CAF–DNA}/i_{CAF} - i_{CAF–DNA}]$ calibration plots)

$$\text{DPV}: \log\left[1/\text{DNA}\right] = 0.9744 \log\left[i_{\text{CAF - DNA}}/i_{\text{CAF}} - i_{\text{CAF - DNA}}\right] + 3.6547,\ R^2 = 0.9799 \quad (19)$$

$$KDV: \log\left[1/DNA\right] = 0.8500 \log\left[i_{\text{CAF - DNA}}/i_{\text{CAF}} - i_{\text{CAF - DNA}}\right] + 3.9366,\ R^2 = 0.9971 \quad (20)$$

The binding ratio of CAF–DNA complexes is 1:1 for both DPV and SWV techniques. Using the DPV and SWV techniques, the calculated $K_{CAF–DNA}$ values are 4.52 $(\pm 1.06)\times 10^3\ M^{-1}$ and 8.64 $(\pm 0.08)\times 10^3\ M^{-1}$, respectively. These results indicate that the binding of CAF to DNA is not in intercalation mode. The CAF–DNA complex formation is controlled by weak electrostatic forces. Calculated $\Delta G^0$ values for DPV and SWV are – 20.85 and – 23.29 kJ/mole, respectively, indicating that CAF–DNA complex formation is thermodynamically spontaneous. These results are compatible with the literature data that studied this interaction with UV-spectroscopy (Nafisi et al. 2008; Johnson et al. 2012).

## Conclusions

A bare pencil graphite electrode was implemented as an electrochemical sensor for the direct determination of caffeine in cola and energy drink samples. In terms of developed DPV and SWV methods, lower concentrations are measured with SWV. However, lower LOD values were obtained with DPV, demonstrating that the DPV method gives more precise current values. Besides, both methods effectively achieved real-sample studies without any pre-treatment or modification.

Caffeine is located in samples of food and drug technology interest. Its interaction with DNA is governed by weak electrostatic forces, and the nature of the interaction is thermodynamically spontaneous according to the calculated binding constants and Standard Free Gibbs Energy Change values, respectively.

**Supplementary Information** The online version contains supplementary material available at https://doi.org/10.1007/s11696-022-02580-8.

**Acknowledgments** We are thankful to the Ankara University Research Fund for financial support on the project number 20L0430001.

## Declarations

**Conflict of interest** The authors declare that there are not any conflicts of interest.

## References

Aklilu M, Tessema M, Redi-Abshiro M (2008) Indirect voltammetric determination of caffeine content in coffee using 1,4-benzoquinone modified carbon paste electrode. Talanta 76(4):742–746. https://doi.org/10.1016/j.talanta.2008.04.042

Alizadeh T, Ganjali MR, Zare M, Norouzi P (2010) Development of a voltammetric sensor based on a molecularly imprinted polymer (MIP) for caffeine measurement. Electrochim Acta 55(5):1568–1574. https://doi.org/10.1016/j.electacta.2009.09.086

Anvari L, Ghoreishi SM, Faridbod F, Ganjali MR (2021) Electrochemical determination of methamphetamine in human plasma on a nanoceria nanoparticle decorated reduced graphene oxide (rGO) glassy carbon electrode (GCE). Anal Lett 54(15):2509–2522. https://doi.org/10.1080/00032719.2021.1875229

Bayraktepe DE (2020) A voltammetric study on drug-dna interactions: kinetic and thermodynamic aspects of the relations between the anticancer agent Dasatinib and Ds-DNA using a pencil lead

graphite electrode. Microchem J 157:104946. https://doi.org/10.1016/j.microc.2020.104946
Bayraktepe DE, Yazan Z, Polat K (2016) Sensitive and selective voltammetric determination of anti-cancer agent shikonin on sepiolite clay/TiO2 nanoparticle/MWCNTs composite carbon paste sensor and investigation of its electro-oxidation mechanism. J Electroanal Chem 780:38–45. https://doi.org/10.1016/j.jelechem.2016.08.035
Bayraktepe DE, İnal EK, Yazan Z (2021) Preparation and characterization of a pencil graphite electrode modified with gold nanoparticles decorated poly (l-methionine) and its use in the simultaneous sensitive electrochemical analysis of ascorbic acid, acetaminophen, chlorpheniramine maleate, and caffeine. Microchem J 171:106812. https://doi.org/10.1016/j.microc.2021.106812
Berman NK, Honig S, Cronstein BN, Pillinger MH (2022) The effects of caffeine on bone mineral density and fracture risk. Osteoporos Int. https://doi.org/10.1007/s00198-021-05972-w
Caldecott KW, Ward ME, Nussenzweig A (2022) The threat of programmed DNA damage to neuronal genome integrity and plasticity. Nat Genet 54:115–120. https://doi.org/10.1038/s41588-021-01001-y
Choi W, Lee ES (2022) Therapeutic targeting of DNA damage response in cancer. Int J Mol Sci 23:1701. https://doi.org/10.3390/ijms23031701
Eisele APP, Valezi CAF, Sartori ER (2017) Exploiting the high oxidation potential of carisoprodol on a boron-doped diamond electrode: an improved method for its simultaneous determination with acetaminophen and caffeine. Analyst 142:3514–3521. https://doi.org/10.1039/C7AN01074E
Erdem A, Ozsoz M (2002) Electrochemical DNA biosensors based on DNA-drug interactions. Electroanalysis 14(14):965–974. https://doi.org/10.1002/1521-4109(200208)14:14%3c965::AID-ELAN965%3e3.0.CO;2-U
Fekry RA, Kelani KM, Fayez YM, Tantawy MA (2022) Comparative validated chromatographic methods for the simultaneous determination of cafeine, codeine, paracetamol along with the related compound "p-aminophenol" in tablets. J Planar Chromatogr Mod TLC. https://doi.org/10.1007/s00764-022-00150-y
Ferrag C, Noroozifar M, Kerman K (2020) Thiol functionalized carbon ceramic electrode modified with multi-walled carbon nanotubes and gold nanoparticles for simultaneous determination of purine derivatives. Mater Sci Eng C 110:110568. https://doi.org/10.1016/j.msec.2019.110568
Fitoz A, Yazan Z, Önal M (2021) Simultaneous trace electrochemical determination of xanthine theophylline and theobromine with a novel sensor based on a composite including metal oxide nanoparticle multi-walled carbon nanotube and nano-Na-montmorillonite clay. Electroanalysis 33(10):2226–2234. https://doi.org/10.1002/elan.202100196
Geto A, Brett CMA (2021) Electrochemical sensor for caffeine in coffee and beverages using a naphthalene sulfonic acid polymer film-based modified electrode. Food Anal Methods 14:2386–2394. https://doi.org/10.1007/s12161-021-02078-1
Gowda JI, Nandibewoor ST (2014) Simultaneous electrochemical determination of 4-aminophenazone and caffeine at electrochemically pre-treated graphite pencil electrode. Anal Methods 6:5147–5154. https://doi.org/10.1039/c4ay00467a
Habibi B, Abazari M, Pournaghi-Azara MH (2012) A carbon nanotube modified electrode for determination of caffeine by differential pulse voltammetry. Chin J Catal 33(11):1783–1790. https://doi.org/10.1016/S1872-2067(11)60438-5
Habibi B, Abazari M, Pournaghi-Azar MH (2014) Simultaneous determination of codeine and caffeine using single-walled carbon nanotubes modified carbon-ceramic electrode. Colloids Surf B 114:89–95. https://doi.org/10.1016/j.colsurfb.2013.09.026
Ilager D, Malode SJ, Shetti NP (2022) Development of 2D graphene oxide sheets-based voltammetric sensor for electrochemical sensing of fungicide, carbendazim. Chemosphere 303:134919. https://doi.org/10.1016/j.chemosphere.2022.134919
Jadon N, Jain R, Sharma S, Singh K (2016) Recent trends in electrochemical sensors for multianalyte detection: a review. Talanta 161:894–916. https://doi.org/10.1016/j.talanta.2016.08.084
Johnson IM, Prakash H, Prathiba J, Raghunathan R, Malathi R (2012) Spectral analysis of naturally occurring methylxanthines (theophylline, theobromine and caffeine) binding with DNA. PLoS ONE 70(12):e50019. https://doi.org/10.1371/journal.pone.0050019
Kawde AN, Baig N, Sajid M (2016) Graphite pencil electrodes as electrochemical sensors for environmental analysis: a review of features, developments, and applications. RSC Adv 6:91325–91340. https://doi.org/10.1039/C6RA17466C
Klevebrant L, Frick A (2022) Effects of caffeine on anxiety and panic attacks in patients with panic disorder: a systematic review and meta-analysis. Gen Hosp Psychiatry 74:22–31. https://doi.org/10.1016/j.genhosppsych.2021.11.005
Koçak ÇC, Nas A, Kantekin H, Dursun Z (2018) Simultaneous determination of theophylline and caffeine on novel [Tetra-(5-chloroquinolin-8-yloxy) phthalocyanato] manganese(III)-Carbon nanotubes composite electrode. Talanta 184:452–460. https://doi.org/10.1016/j.talanta.2018.03.029
Legraverend M, Grierson DS (2006) The purines: Potent and versatile small molecule inhibitors and modulators of key biological targets. Bioorg Med Chem 14:3987–4006. https://doi.org/10.1016/j.bmc.2005.12.060
Li HH, Aubrecht J, Fornace AJ Jr (2007) Toxicogenomics: overview and potential applications for the study of non-covalent DNA interacting chemicals. Mutat Res 623:98–108. https://doi.org/10.1016/j.mrfmmm.2007.03.013
Ly SY, Jung YS, Kim MH et al (2004) Determination of caffeine using a simple graphite pencil electrode with square-wave anodic stripping voltammetry. Microchim Acta 146:207–213. https://doi.org/10.1007/s00604-004-0209-3
Mahanthappa M, Yellappa S, Kottam N, Vusa CSR (2016) Sensitive determination of caffeine by copper sulphide nanoparticles modified carbon paste electrode. Sens Actuators A 248:104–113. https://doi.org/10.1016/j.sna.2016.07.013
Mahnashi MH, Mahmoud AM, Alkahtani SA, Ali R, El-Wekil MM (2020) Facile fabrication of a novel disposable pencil graphite electrode for simultaneous determination of promising immunosuppressant drugs mycophenolate mofetil and tacrolimus in human biological fluids. Anal Bioanal Chem 412:355–364. https://doi.org/10.1007/s00216-019-02245-8
Mekassa B, Tesseman M, Chandravanshi BS (2017) Simultaneous determination of caffeine and theophylline using square wave voltammetry at poly(L-aspartic acid)/functionalized multi-walled carbon nanotubes composite modified electrode. Sens Bio-Sens Res 16:46–54. https://doi.org/10.1016/j.sbsr.2017.11.002
Monteiro MKS et al (2019) Novel cork-graphite electrochemical sensor for voltammetric determination of caffeine. J Electroanal Chem 839:283–289. https://doi.org/10.1016/j.jelechem.2019.03.030
Mukherjee A, Sasikala WD (2013) Chapter one - drug–DNA intercalation: from discovery to the molecular mechanism. Adv Protein Chem Struct Biol 92:1–62. https://doi.org/10.1016/B978-0-12-411636-8.00001-8
Nafisi S, Manouchehri F, Tajmir-Riahi HA, Varavipour M (2008) Structural features of DNA interaction with caffeine and theophylline. Mol Struct 875(3):392–399. https://doi.org/10.1016/j.molstruc.2007.05.010
Neef AB, Samain F, Luedtke NW (2012) Metabolic labeling of DNA by purine analogues in vivo. ChemBioChem 13:1750–1753. https://doi.org/10.1002/cbic.201200253

Nia NA, Foroughi MM, Jahani S (2021) Simultaneous determination of theobromine, theophylline, and caffeine using a modified electrode with petal-like $MnO_2$ nanostructure. Talanta 222:121563. https://doi.org/10.1016/j.talanta.2020.121563

Patel BR, Imran S, Ye W, Weng H, Noroozifar M et al (2020) Simultaneous voltammetric detection of six biomolecules using a nanocomposite of titanium dioxide nanorods with multi-walled carbon nanotubes. Electrochim Acta 362:137094. https://doi.org/10.1016/j.electacta.2020.137094

Rauf S et al (2005) Electrochemical approach of anticancer drugs–DNA interaction. J Pharm Biomed Anal 37(2):205–217. https://doi.org/10.1016/j.jpba.2004.10.037

Rezaei B, Boroujeni MK, Ensafi AA (2014) Caffeine electrochemical sensor using imprinted film as recognition element based on polypyrrole, sol-gel, and gold nanoparticles hybrid nanocomposite modified pencil graphite electrode. Biosens Bioelectron 60:77–83. https://doi.org/10.1016/j.bios.2014.03.028

Sarakhman O, Benkov A, Svorc L (2022) A modern and powerful electrochemical sensing platform for purines determination: Voltammetric determination of uric acid and caffeine in biological samples on miniaturized thick-film boron-doped diamond electrode. Microchem J 175:107132. https://doi.org/10.1016/j.microc.2021.107132

Shokrzadeh M, Hosseinzadeh MH, Boustani M, Habibi E (2022) Determination of caffeine, total phenol, and heavy metals content in green and black tea collected from Gilan Province, Iran by spectroscopic method. PBR 8(1):23–30

Sirajuddin M, Ali S, Badshah A (2013) Drug–DNA interactions and their study by UV– Visible, fluorescence spectroscopies and cyclic voltametry. J Photochem Photobiol B 124:1–19. https://doi.org/10.1016/j.jphotobiol.2013.03.013

Soto C, Ponce-Rodríguez HD, Verdú-Andrés J, Herráez-Hernández R, Campíns-Falcó P (2022) Determination of caffeine in dietary supplements by miniaturized portable liquid chromatography. J Chromatogr A 1664:462770. https://doi.org/10.1016/j.chroma.2021.462770

Švorc L, Tomčík P, Svítková J, Rievaj M, Bustin D (2012) Voltammetric determination of caffeine in beverage samples on bare boron-doped diamond electrode. Food Chem 135(3):1198–1204. https://doi.org/10.1016/j.foodchem.2012.05.052

Svorc L (2013) Determination of caffeine: a comprehensive review on electrochemical methods. Int J Electrochem Sci 8:5755–5773

Svorc L, Haššo M, Sarakhman O, Kianičková K, Stanković DM et al (2018) A progressive electrochemical sensor for food quality control: reliable determination of theobromine in chocolate products using a miniaturized boron- doped diamond electrode. Microchem J 142:297–304. https://doi.org/10.1016/j.microc.2018.07.007

Torres AC, Barsan MM, Brett CMA (2014) Simple electrochemical sensor for caffeine based on carbon and Nafion-modified carbon electrodes. Food Chem 149:215–220. https://doi.org/10.1016/10.1016/j.foodchem.2013.10.114

Tran BT, Tran TN, Tran AMT, Nguyen GCD, Nguyen QTT (2022) simultaneous determination of paracetamol, ibuprofen, and caffeine in tablets by molecular absorption spectroscopy combined with classical least square method. Molecules 27:2657. https://doi.org/10.3390/molecules27092657

Vieira LR, Soares AMVM, Freitas R (2022) Caffeine as a contaminant of concern: a review on concentrations and impacts in marine coastal systems. Chemosphere 286:131675. https://doi.org/10.1016/j.chemosphere.2021.131675

Wong A et al (2021) Simultaneous determination of direct yellow 50, tryptophan, carbendazim, and caffeine in environmental and biological fluid samples using graphite pencil electrode modified with palladium nanoparticles. Talanta 222:121539. https://doi.org/10.1016/j.talanta.2020.121539

Yazan Z, Bayraktepe DE, Dinç E (2020) Four-way parallel factor analysis of voltammetric four-way dataset for monitoring the etoposide-DNA interaction with its binding constant determination. Bioelectrochemistry 134:107525. https://doi.org/10.1016/j.bioelechem.2020.107525

Zereykaya B, Bayraktepe DE, Yazan Z (2020) An adsorptive stripping voltammetric study based on disposable pencil graphite sensor for the determination of caffeine in local brand ice tea. Cumhur Sci J 41(3):680–689. https://doi.org/10.17776/csj.740556

Zhang J, Wang LP, Guo W, Peng XD, Li M et al (2011) Sensitive differential pulse stripping voltammetry of caffeine in medicines and cola using a sensor based on multi-walled carbon nanotubes and nafion. Int J Electrochem Sci 6:997–1006

**Publisher's Note** Springer Nature remains neutral with regard to jurisdictional claims in published maps and institutional affiliations.

Springer Nature or its licensor (e.g. a society or other partner) holds exclusive rights to this article under a publishing agreement with the author(s) or other rightsholder(s); author self-archiving of the accepted manuscript version of this article is solely governed by the terms of such publishing agreement and applicable law.